PCCP

Accepted Manuscript

This is an *Accepted Manuscript*, which has been through the Royal Society of Chemistry peer review process and has been accepted for publication.

Accepted Manuscripts are published online shortly after acceptance, before technical editing, formatting and proof reading. Using this free service, authors can make their results available to the community, in citable form, before we publish the edited article. We will replace this *Accepted Manuscript* with the edited and formatted *Advance Article* as soon as it is available.

You can find more information about *Accepted Manuscripts* in the Information for Authors.

Journal Name

ROYAL SOCIETY OF CHEMISTRY

ARTICLE TYPE

Properties of theranostic nanoparticles determined in suspension by ultrasonic spectroscopy†

Ksenia Astafyeva,[a,b] Jean-Louis Thomas,[*a] François Coulouvrat,[c] Matthieu Guédra,[c] Odile Diou,[d] Ludivine Mousnier,[d] Nicolas Tsapis,[d] Wladimir Urbach,[b,e,f] and Nicolas Taulier[b]

In the context of a growing use of nanoparticles, it is important to be able to characterize all their physical properties in order to understand their behavior, to optimize them, and to control their quality. We showed that ultrasonic spectroscopy provides many of the desired properties. To do so, we used as an example nanocapsules made of a polymer shell encapsulating a liquid perfluorocarbon core and designed for theranostic applications. Frequency-dependent measurements of both ultrasound velocity and attenuation were performed on nanocapsule suspensions. Then the desired properties were extracted by analyzing the experimental data using a recently developed model that relates the speed of sound and attenuation of a suspension to the geometrical and viscoelastic properties of the nanocapsules.

1 Introduction

The use of nanoparticles is fast growing and reaches many fields, including industrial[1], cosmetic[2], and medical[3,4] applications. These nanoparticles are made of various materials (metals, polymers, lipids, surfactants...) and their optimization for a desired application requires a precise characterization of their properties as they will dictate the nanoparticle behavior and efficiency. However the measurement of the structural, mechanical, and viscoelastic properties of a nanoparticle is difficult as there is no direct and precise method to establish them, given the nanometric size and the fact that particles are used in suspension.

Ultrasonics is already a well-known series of techniques for characterizing the physical properties of emulsions and suspensions. For instance, they have been used to measure volume fraction of dispersed phases[5,6], particle compressibility,[7,8] or size of rigid nanoparticles[9]. However, the interpretation of acoustic measurements requires an appropriate model. Commercial acoustic devices usually use the ECAH model, a well known

acoustic theory for heterogeneous systems first developed by Epstein and Carhart[10], and by Allegra and Hawley[11]. This model describes the attenuation of sound through a dilute suspension of isolated spheres due to thermal and viscous effects, decomposing an acoustic wave in a set of spherical harmonics in a linear regime. Another powerful approach is the coupled phase theory[12,13]. The main difference between the coupled phase and the scattering approaches is that coupled phase theory permits an easier physical interpretation of the obtained equations. Moreover, it allows to take into account more easily some complex phenomena such as non-linearity. Commercial micrometric ultrasound contrast agents with a gaseous core have been successfully described by this theory, with various models generalizing the well-known Rayleigh-Plesset equation of bubble dynamics to account for the mechanical properties of a thin encapsulating shell. The shell can be described either as an incompressible, viscoelastic shell with Kelvin-Voigt[14] or Maxwell-type relaxation rheology[15], or a nonlinear surface tension[16]. On the contrary, for rigid nanoparticles, visco-inertial effects govern their hydrodynamic interactions through the relative motion of particles within the solvent[9], i.e Faxén forces[17,18] associated to the translational motion of the particles. For nanometric but deformable particles both translational motion and dilatational deformation of the particles should be taken into account as they are of comparable order of magnitude[19]. The assumption of shell incompressibility has also been shown irrelevant at the nanometric scale, as shell and liquid core compressibilities are comparable. Despite their sophistication, these models cannot be applied to any kind of nanoparticles, they fail in particular to predict the acoustic be-

[a] Sorbonne Universités, UPMC Univ Paris 06, CNRS-UMR 7588, Institut des NanoSciences de Paris, F-75005, Paris, France.
[b] Sorbonne Universités, UPMC Univ Paris 06, CNRS, INSERM, Laboratoire d'Imagerie Biomédicale, F-75006, Paris, France.
[c] Sorbonne Universités, UPMC Univ Paris 06, CNRS-UMR 7190, Institut Jean Le Rond d'Alembert, F-75005, Paris, France.
[d] Institut Galien Paris-Sud, UMR CNRS 8612, Labex LERMIT, Châtenay-Malabry, France.
[e] LPS de l'ENS, UMR 8550 CNRS, 24 rue Lhomond, F-75005 Paris, France.
[f] Université Paris Descartes, Paris, France.
[*] E-mail: jean-louis.thomas@upmc.fr

havior of polymeric nanocapsule suspensions. To alleviate this problem, an extended model was recently derived by Guédra *et al.*[20] that generalizes the Church model for the dilatation part in the case of compressible shells and polydisperse suspensions.

This model is used in this article to demonstrate that it is possible to derive *in vitro* the geometrical and viscoelastic properties of nanoparticle suspensions using ultrasonic spectroscopy. Note however this method cannot be straightforwardly applied *in vivo* due to the complexity of the sonicated medium. As nanoparticles, we used nanocapsules made of perfluoroctyl bromide (PFOB) encapsulated within a shell of biocompatible and biodegradable polymer poly(lactic-co-glycolic) acid (PLGA). These nanocapsules are intended to be injected intravenously to act as ultrasound[19] or MRI contrast agents as well as drug carriers[21–23]. Their small size allows them to take advantage of the enhanced permeability and retention effect[24,25], which partially leads to a passive accumulation of nanoparticles into tumor tissues[26–29]. But little is known about the physical properties of these nanocapsules which hinders their optimization.

2 Experimental

2.1 Materials

Poly(lactide-co-glycolide) (PLGA) Resomer RG502 (Mn = 10,000 g/mol) was obtained from Boehringer-Ingelheim (Germany). Polyvinyl alcohol (PVA) (Mw = 30,000–70,000, 89% hydrolyzed) and sodium cholate (SC) were purchased from Sigma-Aldrich (France). Perfluoro-octyl bromide (PFOB) was obtained from Fluorochem (UK). Methylene chloride RPE-ACS 99.5% was provided by Carlo Erba Reactifs (France). Water was purified using a Milli-Q system from Merck Millipore (France).

2.2 Preparation of nanocapsule suspensions

Nanocapsules were prepared by an emulsion-evaporation process described in details elsewhere.[21,30] Briefly, PLGA and PFOB were dissolved into methylene chloride and the solution was placed into a thermostated bath at 20°C. The organic solution was then emulsified into 1.5% (w/v) sodium cholate solution with an Ultra-turrax T25 (IKA-Labortechnik, Staufen, Germany) operating with a SN25-10G dispersing tool at 8,000 rpm for 30 s. The primary emulsion was then sonicated with a Vibra cell tip (Bioblock Scientific, France), for 2 mn over ice at 200 W. Methylene chloride was then evaporated by magnetic stirring for 3 h at 300 rpm in a thermostated bath (20°C). In order to replace sodium cholate by PVA, nanoparticle solutions were incubated with 1% (w/v) PVA for five days at 4°C. Afterwards the solutions were washed by centrifugation (10,000 g; 1 h; 4°C) using a MR 1812 centrifuge (Jouan, France). The supernatant containing surfactants was discarded and nanoparticles were resuspended by vortexing with the desired amount of water. The end product of this preparation is a suspension in water of nanocapsules of mean radius R_m that are composed of a liquid PFOB core encapsulated into a PLGA shell of mean thickness T_m. If the addition of PFOB is omitted, nanoparticles are only made of PLGA.

2.3 Size measurements

Size distributions of particle suspensions were measured by dynamic light scattering (DLS) for 60 s at a scattering angle of 173° using a Zetasizer Nano ZS Instrument (Malvern, France). Measurements were performed in triplicate using suspensions diluted in water to avoid multiple scattering. Samples were further filtered through a 0.22 μm membrane to avoid scattering from dust. The data were converted from intensity (scattered intensity vs. particle radius) to number distribution (number of particles vs. particle radius). Thanks to this convertion it was possible to derive a more accurate particle mean radius, R_m, from the size distribution. The polydispersity index, PdI_R, was also derived using the equation

$$PdI_R = \left(\frac{\sigma}{R_m}\right)^2 \tag{1}$$

where σ is the standard deviation of the particle size distribution.

2.4 Volumetric measurements

A digital densitometer Anton Paar DMA 5000 M (Graz, Austria) was used to measure densities at (25 ± 0.01)°C with a precision of 0.005 kg/m³. The device derives the density value of a solution from the measurement of the oscillation period of a vibrating U-tube filled with the solution. The density of a nanocapsule encapsulating PFOB was estimated using the equation:

$$\rho_{nano} = \left[1 - \frac{T_m}{R_m}\right]^3 \times \rho^c + \left(1 - \left[1 - \frac{T_m}{R_m}\right]^3\right) \times \rho^s \tag{2}$$

where ρ^c and ρ^s are respectively the densities of PFOB and PLGA. A value $\rho^c = 1917$ kg/m³ was directly measured from a liquid PFOB sample. The apparent volume of a suspended PLGA nanoparticle is defined as:

$$\phi_{V,PLGA} = \frac{1}{\rho_{aq}} - \frac{\rho - \rho_{aq}}{\rho_{aq}C} \tag{3}$$

where ρ and ρ_{aq} are the densities of a solution of plain PLGA nanoparticles suspended in an aqueous solvent and of the aqueous solvent, respectively. C is the mass concentration of polymer in the solution that has been precisely determined by weighting after sample was lyophilized. The PLGA density $\rho^s = 1/\phi_{V,PLGA}$ can then be directly determined from the equation:

$$\rho^s = \frac{\rho_{aq} \times C}{\rho_{aq} + C - \rho} \tag{4}$$

The measurements gave a value of $\rho^s = 1283$ kg/m³.

Finally, the volume fraction Φ of nanoparticles in a sample is calculated from:

$$\Phi = \frac{\rho - \rho_{aq}}{\rho_{nano} - \rho_{aq}} \tag{5}$$

2.5 Picosecond acoustics

Picosecond ultrasonics was used to determine the high frequency values of the elastic moduli of PLGA in the range 1–10 GHz at 21°C as described in details elsewhere[31]. Briefly, the longitudinal speed of sound in a PLGA film, 2.7 μm thick, was obtained by
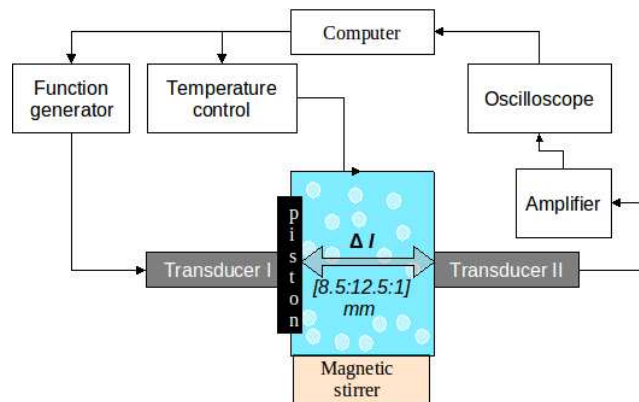
Fig. 1 Schematic representation of the set-up for attenuation and velocity measurements of the ultrasound signal propagated through a suspension. An emitting transducer (I) was used to emit an ultrasound signal that will propagate through the thermostated cell filled with the sample, until it reaches a second transducer (II), with identical characteristics to transducer I. The received signal is then amplified and converted into an electric signal. The measurements were repeated by changing the distance Δl between transducers from 8.5 to 12.5 mm (with a step of 1 mm). The interpolation with Δl of the phase and amplitude of the received signal provided absolute measurements of ultrasound speed and attenuation. These measurements were performed for each of the five transducers, each excited with a broad-band wave centered at 5, 10, 21, 45 or 75 MHz.

Brillouin scattering, while the shear wave speed of sound was estimated from the dispersion curve of Rayleigh surface waves.

2.6 Experimental set-up for ultrasonic spectroscopy

Broadband (from 3 to 90 MHz) ultrasonic measurements of attenuation and longitudinal speed of sound within nanoparticle suspensions were performed in a custom-designed setup (depicted in Figure 1). The setup contains a stainless steel cell with an external parallelepiped shape of $23 \times 60 \times 60$ mm^3. The whole cell is maintained at a constant temperature of 25.6°C (with a precision of 0.1°C) by a thermoelectric heating using the Peltier effect and a PID (proportional-integral-derivative) controller. The cell possesses two optical windows of 6 mm thick facing one another. Two identical transducers (Sofranel, France) were placed in both windows, one of them lined up at the centre of a moving piston and the other one fixed on the opposite side of the cell. The piston motion is controlled by a micrometer with a precision of 1 μm. Thus the distance between the two transducers can be reduced by simply moving the piston that will push the transducer deeper into the cell. Alignment was controlled by minimizing the time-of-flight between the two transducers. Five sets of coupled transducers covering a bandwidth of 3–90 MHz were systematically used. A broadband pulse of 2.5 V amplitude and with a central frequency of 5, 10, 21, 45 or 75 MHz depending of the transducer type was emitted by one transducer using a Tektronix AFG3251 Arbitrary/Function generator. After propagating through the sample, the pulse wave was received by the second transducer. The received signal was amplified by a power amplifier (Booster Amplifier, Precision Acoustics LTD) and digitized using an oscilloscope (Tektronix TDS 5104). At high frequencies

(40–90 MHz) and for the most concentrated nanocapsules suspensions (with a volume fraction of 3%), an additional amplifier (Amplifier Research 150A100B) was used to increase 10 times the amplitude of the emitted signal. During experiments, the suspensions were continuously stirred to homogenize temperature and prevent sedimentation. For each sample, five measurements were performed every 1 mm for a separating distance between transducers varying from 12.5 to 8.5 mm. For each sample, measurements were repeated 100 (for 5 – 45 MHz bandwidth) or 250 (45–90 MHz bandwidth) times, and then time signals were averaged. The higher number of data at higher frequencies was necessary to compensate for the poorer signal-to-noise ratio due to increased attenuation. Finally a Fourier transform was applied on the averaged signal. For each frequency, the linear interpolation of the phase behavior at the 5 piston positions provided the speed of sound, while the linear interpolation of the logarithm of the amplitude yielded the attenuation. The reproducibility and precision of our ultrasonic measurements were checked on pure water at 25 and 37°C. The resolution was 1–2 m/s for speed of sound and 10% for ultrasonic attenuation. The advantage in using a controlled and variable path of propagation is to rely only on the accuracy of the piston position which yields absolute values. However our approach assumes the propagation of a plane wavefront. To assess this assumption, a 3D numerical simulation based on angular spectrum method was carried out, for the whole layered set-up: transducers, glass windows, homogeneous solution, glass windows, and transducer. The simulation results showed that diffraction corrections due to the finite lateral dimensions of the set-up was negligible.

3 Results and Discussion

3.1 Modeling ultrasonic properties of nanoparticle solutions

Recently, Guédra *et al.* developed a model to predict the ultrasonic properties of nanoparticles, such as those studied here, from their geometrical and viscoelastic properties.[20] Since this model will be used in our analysis, we provide hereafter the final theoretical expressions derived from the model and used in our calculations. We consider spherical particles with a core of mean radius, r_m, surrounded by an elastic shell of external mean radius, R_m. The thickness shell is then $T_m = R_m - r_m$. The model also takes into account the polydispersities $n(R)$ and $n(r)$ in both particle radius and thickness, respectively. The volume fraction is noted Φ. To distinguish the different properties of a nanoparticle, superscripts s and c are used when referring to the particle shell and core, respectively, while parameters without a superscript are for nanocapsule suspensions. K and G stand for bulk and shear elastic moduli, while ζ and μ are their viscous counterparts. Assuming a plane wavefront, the speed of sound, c, and attenuation, α, of a suspension are related to the wave number, k, by:

$$k = \frac{\omega}{c} + i \times \alpha \qquad (6)$$

where ω is the ultrasonic wave frequency. The dispersion relation (Equation 6) involves two scattering contributions, the first one, $I(r_m, R_m, \omega)$, describes the visco-inertial dipolar contribution while the second one, $D(r_m, R_m, \omega)$, is a monopolar dilatational

term. Taking $\hat{k}$ as the wave number in the solvent, the dispersion relation writes as:

$$\left(\frac{k}{\hat{k}}\right)^2 = \left(\frac{1-\Phi}{1-i\omega\tau_V\frac{1-D(r_m,R_m,\omega)}{1+I(r_m,R_m,\omega)}}\right)(1-D(r_m,R_m,\omega))\left(\frac{1+\tilde{\rho}(r_m,R_m,\omega)I(r_m,R_m,\omega)}{1+I(r_m,R_m,\omega)}\right) \quad (7)$$

where

$$\tau_V = \frac{1}{\rho_{aq}c_{aq}^2}\left(\zeta_{aq}+\frac{4}{3}\mu_{aq}\right) \quad (8)$$

is the characteristic time associated to solvent viscous absorption and ρ_{aq} is the density of aqueous solvent. The monopolar dilatational term, $D(r_m,R_m,\omega)$, comes from the linearization of a Rayleigh-Plesset like equation:

$$D(r_m,R_m,\omega) = \frac{\rho_{aq}c_{aq}^2}{1-\Phi}\iint\frac{4\pi R^2}{C(r,R,\omega)}n(r)n(R)drdR \quad (9)$$

with

$$C(r,R,\omega) = \omega^2\rho_{aq}R\left(1+i\omega\frac{R}{c_{aq}}\right) - 3\frac{K^c-i\omega\zeta^c}{\chi R}\left(\frac{R}{r}\right)^3$$
$$-4\frac{G^s-i\omega\mu^s}{\chi R}\left(\left(\frac{R}{r}\right)^3-\chi\right)+4i\frac{\omega}{R}\mu_{aq} \quad (10)$$

The quantity χ is equal to 1 for incompressible shell, otherwise:

$$(\chi-1) = \frac{R^3-r^3}{r^3}\times\frac{K^c-i\omega\zeta^c+\frac{4}{3}[G^s(\omega)-i\omega\mu^s(\omega)]}{K^s-i\omega\zeta^s+\frac{4}{3}[G^s(\omega)-i\omega\mu^s(\omega)]} \quad (11)$$

The elastic polymer shell can be modeled by a rheological model. The standard or Zener model is used as it involves only three parameters (the elastic moduli at infinite, G_∞^s, and zero, G_0^s, frequencies, and the relaxation angular frequency ω_r):

$$G^s(\omega) = G_0^s+(G_\infty^s-G_0^s)\frac{(\omega/\omega_r)^2}{1+(\omega/\omega_r)^2} \quad (12)$$

$$\mu^s(\omega) = \frac{G_\infty^s-G_0^s}{\omega_r(1+(\omega/\omega_r)^2)} \quad (13)$$

To avoid introducing additional unknown parameters, we considered that the longitudinal speed of sound, c^s, is frequency independent (as suggested by experimental data, see Table 2) and that the bulk viscosity is relatively small and proportional to shear viscosity, thus:

$$K^s = (c^s)^2\rho^s-\frac{4}{3}G^s \quad (14)$$

$$\frac{\zeta^s}{\mu^s} = \theta \quad (15)$$

where θ a proportionality constant.

The viscous-inertial term, $I(r_m,R_m,\omega)$, is due to Faxén forces and writes as:

$$I(r_m,R_m,\omega) = \frac{1}{1-\Phi}\iint\frac{4}{3}\pi R^3 W(r,R,\omega)n(r)n(R)drdR \quad (16)$$

with

$$W(r,R,\omega) = \frac{F_B(R,\omega)+F_A(R,\omega)}{F_B(R,\omega)+\tilde{\rho}_P(r,R,\omega)F_A(R,\omega)} \quad (17)$$

where $\tilde{\rho}_P(r,R,\omega) = \frac{\rho_{nano}(r,R,\omega)}{\rho_{aq}}$, In equation 17, the steady Stokes and Basset-Boussinesq historical viscous drag forces, along with the inertial added mass effect, are respectively described by:

$$F_B(R,\omega) = 6\pi R\mu_{aq}+3\pi\sqrt{2\rho_{aq}\mu_{aq}\omega}R^2(1-i)-\frac{2}{3}\pi R^3\rho_{aq}i\omega \quad (18)$$

while the Archimedes force is:

$$F_A(R,\omega) = -\frac{4}{3}\pi R^3\rho_{aq}i\omega \quad (19)$$

Finally, in Equation 7, $\tilde{\rho}$ is equal to:

$$\tilde{\rho}(r_m,R_m,\omega) = \frac{\rho_A(r_m,R_m,\omega)}{(1-\Phi)\rho_{aq}I(r_m,R_m,\omega)} \quad (20)$$

where $\rho_A(r_m,R_m,\omega)$ is an apparent complex and frequency-dependent density associated to the motion relative to the ambient fluid of nanoparticles of mass $m_{nano}(r,R)$:

$$\rho_A(r_m,R_m,\omega) = \iint m_{nano}(r,R)W(r,R,\omega)n(r)n(R)drdR \quad (21)$$

We emphasize that many of the involved parameters are temperature dependant, in particular attenuation and sound velocity.

3.2 Nanocapsule suspensions

Four types of nanoparticles were prepared with different amounts of PLGA and PFOB in order to obtain four thickness-to-radius ratios denoted as $(T_m/R_m)_1$ for the thinnest shell (obtained with the smallest content of PLGA), $(T_m/R_m)_2$ that is an intermediate shell thickness, $(T_m/R_m)_3$ for the thickest shell, and finally, $(T_m/R_m)_4 = 1$ corresponding to a plain nanoparticle (*i.e.* with no PFOB). DLS measurements were used to derive the mean radii of each solution type (see Table 1). A mean outer radius, R_m, of 45, 42, 63, and 72 nm was measured for nanocapsules with $(T_m/R_m)_1$, $(T_m/R_m)_2$, $(T_m/R_m)_3$, and plain nanoparticles, respectively. Transmission electron microscopy (TEM) was used in a previous work[30] to estimate the mean polymeric shell thickness T_m. Using these data in combination with our DLS data we obtain the following ratio values: $(T_m/R_m)_1 = 0.25$, $(T_m/R_m)_2 = 0.35$, and $(T_m/R_m)_3 = 0.54$. Finally, Φ values were calculated using Equation 2 and the ratio T_m/R_m determined by TEM, denoted as $(T_m/R_m)^{TEM}$ (see in Table 1).

Table 1 Values of geometrical parameters. External mean radii R_m with its polydispersity index PdI_R were determined from DLS measurements for the four types of nanoparticles. The relative thicknesses $(T_m/R_m)^{TEM}$ were derived from TEM measurements and were used to calculate the volume fraction, Φ, of nanocapsules in solution. The relative thickness, $(T_m/R_m)^{fit}$, and thickness polydispersity, PdI_T^{fit}, were derived from the fit of the our ultrasonic (US) experimental data where R_m was set to the values determined by DLS. Finally, the nanocapsule volume fraction ϕ^{fit} was calculated based on $(T_m/R_m)^{fit}$ values

Suspension	R_m (nm) ± 5 (DLS)	PdI_R (DLS)	$(T_m/R_m)^{TEM}$ ± 0.05 (TEM)	$(T_m/R_m)^{fit}$ (US)	PdI_T^{fit} (US)	Φ (%) ± 0.05 (DLS+TEM)	Φ^{fit} (%) (DLS+US)
$(T_m/R_m)_1$	45	0.2	0.25	0.09	0.02	0.54	0.38
$(T_m/R_m)_2$	42	0.12	0.35	0.25	0.04	0.56	0.47
$(T_m/R_m)_3$	63	0.11	0.54	0.54	0.08	0.60	0.60
$(T_m/R_m)_4$	72	0.08	1	1	0	0.67	0.70

3.3 Typical ultrasonic spectra measurements

In the case of propagation of an ultrasound wave through a classical liquid system (like water), the attenuation coefficient satisfies a quadratic law with frequency while the speed of sound value is independent of frequency in the 3–90 MHz range. For comparison, Figure 2 presents an example of attenuation and sound velocity measurements in a nanocapsule suspension at a volume fraction of 3%. In this example the nanocapsules possess a PFOB core with the thinnest PLGA shell among our samples, *i.e.* with a $(T_m/R_m)_1$ ratio. The figure displays a general typical behavior observed for all our other samples. Specifically, as the frequency increases, we observe a roughly linear growth of the attenuation coefficient, while the values of speed of sound decrease at low frequencies. At low frequency, a dispersion is clearly detected in both ultrasonic spectra of Figure 2 with an inflection point located around 12 MHz. The speed of sound curve exhibits discontinuities because the velocity magnitude is affected by the unperfect alignment between the two transducers and by the piston position accuracy occuring when changing transducers. But these discontinuities do not affect the overall variation of the curves.

3.4 Reduction of unknown parameters

The model described previously uses 16 parameters, noted as Φ, r_m, R_m, $n(r)$, $n(R)$, $m_P(r,R)$, ρ_{aq}, c^s, K^c, K^s, ζ^c, θ, G_0^s, and G_∞^s. A fit of our data with so many unknown parameters would lead to an inaccurate estimation of these parameters. So the first step should be devoted to the reduction of this number.

We recall that the volume fraction Φ of nanoparticle was estimated using Equation 5 based on the density values of PLGA and PFOB (see Table 2), and on thickness-to-radius ratio $(T_m/R_m)^{TEM}$ provided by TEM (Table 1). $m_P(r,R)$ is easily calculated as we know the mass of the nanoparticle shell and core. The properties of the solvent, e.g ρ_{aq}, are also known or can be easily measured. As r_m and R_m are mean values, they also correspond to the mean value derived from the integration of the size distribution of the inner and outer radius $n(r)$ and $n(R)$, respectively. The size distribution of R has been directly measured by light scattering. Two examples are displayed in Figure 3 for PLGA plain nanoparticles, *i.e.* $(T/R)_4 = 1$, and nanoparticles with the thinnest shell, *i.e.* $(T/R)_1$. Whatever the type of nanoparticle, the size distribution is always right skewed with a polydipersity index equal to $PdI_R = 0.08 \pm 0.01$ for plain particle whereas parti-

Table 2 Values of material parameters. ρ represents the density values measured at 25 °C. The speed of sound c (compression waves) was measured at 25 °C and at a frequency ranging from 3 to 90 MHz, except for PLGA that was determined from picosecond ultrasonics measurements. The other parameters are the bulk modulus K, shear modulus G, dynamic viscosity μ, and bulk viscosity ζ of nanoparticle components and solvents. The PFOB bulk viscosity was calculated from the attenuation spectrum using the shear viscosity found in literature [32]. Data for water are standard. Viscoelastic properties are taken from litterature and * is from picosecond ultrasonics measurements

	Solvent		Shell	Core
Material	Water	Sodium cholate	PLGA	PFOB
ρ (kg/m³)	997	1001	1283	1917
C (m/s)	1498	1505	2370*, 2326[33], 2400[34]	623
K (GPa)	2.2	2.3	7.3*	0.74
G (GPa)	0	0	1.6*	0
μ (m Pa s)	1	1	-	2
ζ (m Pa s)	2.4	2.4	-	7.2

cles possessing a liquid core always exhibit a polydipersity index of $PdI_R = 0.2 \pm 0.01$. These size distributions can be well fitted using a log-normal distribution and this last fit function was used as $n(R)$. The size distribution of the internal radius is unknown. We decided to use for $n(r)$ a log-normal distribution with a zero probability at $r = 0$ (as PFOB should be present) and truncated at $r = R$ with an unknown polydispersity index PdI_r. Thus $n(R)$ only depends on R while $n(r)$ depends on R and PdI_r in addition to r.

We know from our model that the resonance frequency of the nanoparticle shell, ω_r, is responsible of the inflection observed in both the attenuation and sound velocity curves, thus $\omega_r = 12$ MHz.

The elastic properties at infinite frequency of the PLGA shell were derived from picosecond ultrasonic techniques. We measured $G_\infty^s = 1.6$ GPa and $K_\infty^s = 7.3$ GPa. This leads to a Young modulus E_∞^s equal to 4.3 GPa, and a Poisson's ratio v_∞ equal to 0.36. Poisson's ratio significantly departs from the incompressible limit 0.5, showing that PLGA cannot be considered as a rubber-like material with $G^S \ll K^S$. These values correspond to a longitudinal speed of sound equal to $c^s = 2370$ m/s, similar to values measured by Parker *et al.* [33] (2326 m/s) at 10 MHz and by Dehoux *et al.* (2400 m/s) at 1 GHz [34]. At low frequencies, literature data are scarce and provide Young's modulus varying from 0.6 to 4.4 GPa using different techniques as well as different monomers ratio and molecular weights for PLGA. [35–39] For a copolymer similar to the
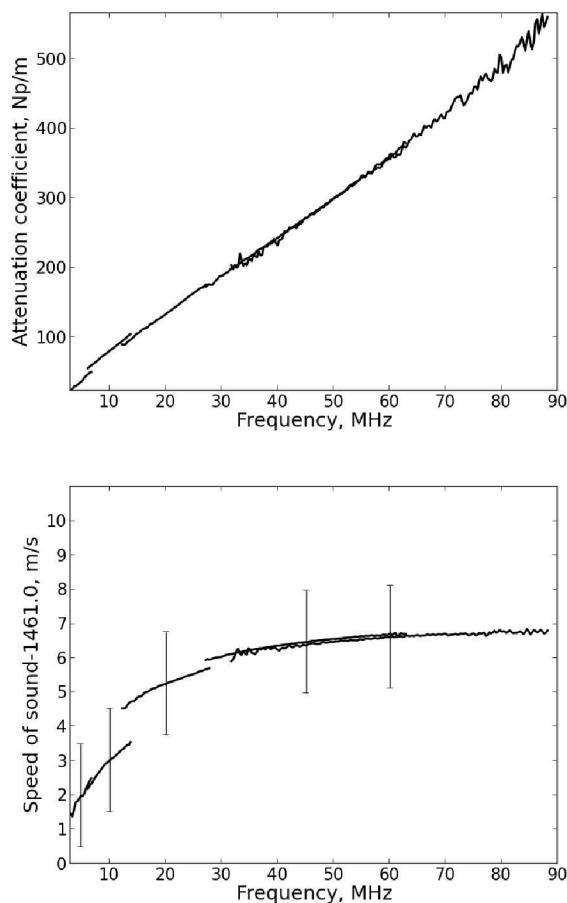
Fig. 2 Variation of the attenuation coefficient and speed of sound measured for a volume fraction of 3% of a suspension containing nanoparticles with the thinnest shell (i.e. $(T_m/R_m)_1$). Precisions in the attenuation and c measurements were 10% and 2 m/s, respectively, in all the frequency range.

Fig. 3 Size distribution (percentage of a population calculated in number) of plain PLGA nanoparticles (solid line) and the thinnest (i.e. $(T/R)_1$) PLGA-PFOB nanocapsules (dashed line).

and a volume fraction $\Phi = 0.5\%$. The model was used to draw curves with a ratio θ varying from 0 to 3. It appears that the magnitude of the ultrasound attenuation is proportional to the bulk-to-shear viscosities ratio θ. The model was in good agreement with the experimental spectra (i.e. minimized residuals) for the values 0.25 and 0.5. In the following we choose $\theta = \zeta^s/\mu^s = 0.5$ and we expect this value to be the same in the presence of the PFOB core.

Finally, for nanoparticles encapsulating a PFOB core, the only remaining unknown values were r_m and PdI_r. These values are difficult to obtain by conventional techniques. We could derive values for $r_m = R_m - T_m$ based on TEM measurements, but an accurate estimation of shell thickness was difficult because of a low contrast detected in TEM between the compounds. Thus we consider this parameter as unknown for now.

PLGA used for our nanoparticles (i.e. $PGA : PLA = 50\!:\!50$), previous studies provided a value about 1.3 GPa[37–39]. Thus, using this value and the Poisson's ratio obtained from picosecond measurements ($\nu_\infty = 0.36$), we estimated the shear modulus at zero frequency to be $G_0^s = 0.48$ GPa.

The sound velocity, c^c, and attenuation, α^c, were measured for a solution of PFOB. Using these values and the PFOB density, ρ^c, we obtain for PFOB the bulk modulus:

$$K^c = \rho^c c^{c2} \tag{22}$$

and the bulk viscosity:

$$\zeta^c = \frac{2\rho^c c^{c3}}{\omega^2}\alpha^c - \frac{4}{3}\mu^c \tag{23}$$

At this stage, the unknown parameters were easily reduced to r, PdI_r, and θ. Considering PLGA plain nanoparticles (i.e. $(T/R)_4 = 1$), this list is reduced to $\theta = \zeta^s/\mu^s$ as we do not consider the integration of r in the model's equation. Figure 4 presents the experimental curve for the measured attenuation of a suspension of PLGA plain nanoparticles with a mean radius of $R = 72 \pm 5$ nm
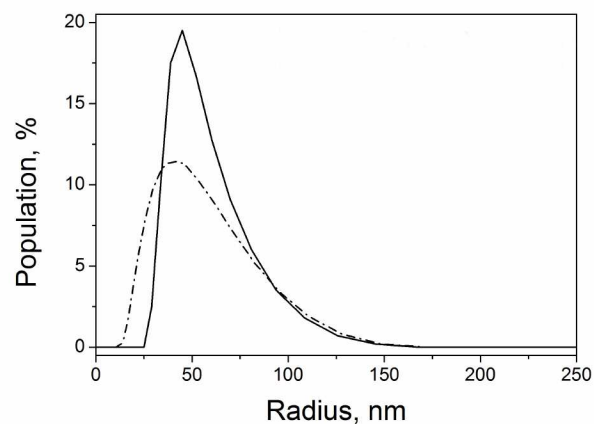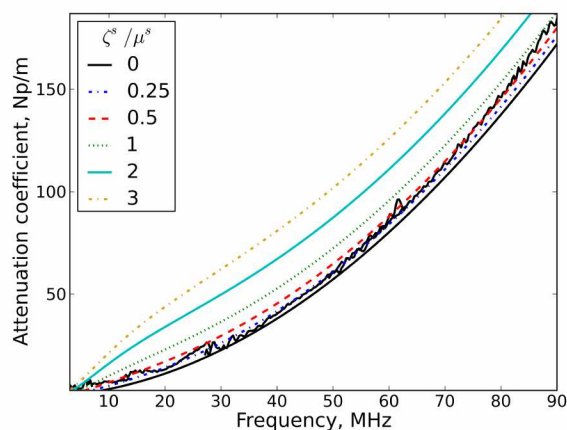

Fig. 4 Comparison of the theoretical model varying the bulk viscosity of the PLGA shell to the attenuation experimental spectrum. Several bulk-to-shear viscosities ratios were considered: $\zeta^s/\mu^s = 0$ (solid black), 0.25 (dotted blue), 0.5 (dashed red), 1 (dotted green), 2 (solid cyan), and 3 (dotted goldenrod). Noisy black curve is experimental one, smooth curves are model ones.

3.5 Determination of the inner core radius and shell thickness

We used the model of Guédra *et al.* to fit the attenuation and speed of sound curves for solutions of nanocapsules with a PFOB core where r_m and PdI_r were the only unknown parameters. The values of all the other parameters are given in Tables 1 and 2. The model fitted with a good accuracy the experimental data as shown in Figure 5. The polydipersities of r and R, respectively derived from the ultrasonic data fit and measured by DLS, were used to calculate the polydispersity in thickness PdI_T^{fit} as given in Table 1. From these fits: $(T_m/R_m)_1^{fit} = 0.09$, $(T_m/R_m)_2^{fit} = 0.25$, and $(T_m/R_m)_3^{fit} = 0.54$. Recall that TEM measurements estimated these
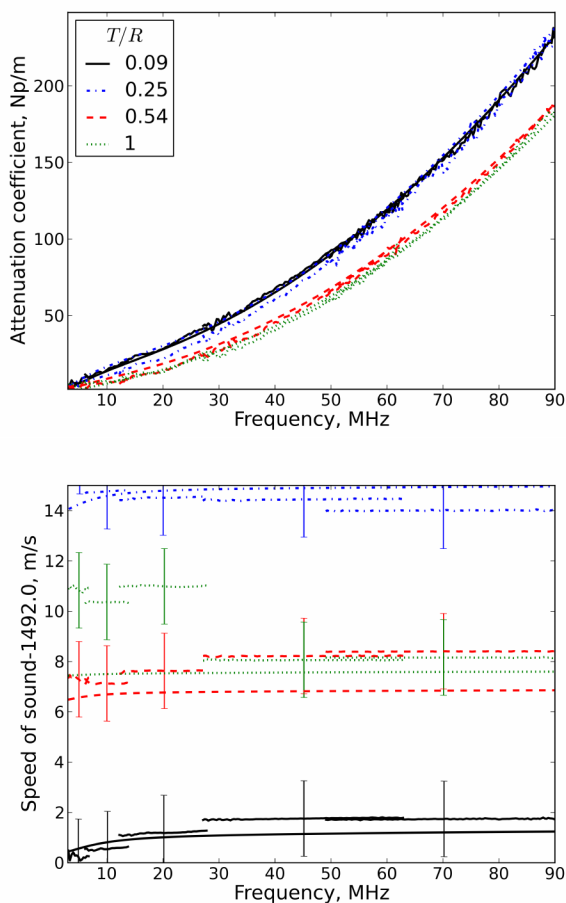

Fig. 5 Comparison of the theoretical model including compressibility to the response from PLGA-PFOB particles of different thickness. Three relative thicknesses were considered: $T_m/R_m = 0.09$ (black), 0.25 (blue), 0.54 (red), and 1 (green). The $T_m/R_m = 0.25$ data were measured in another solvent (1.5% w./v. sodium cholate). Noisy curves are experimental ones, smooth curves are model ones.

ratios to be 0.25, 0.35, and 0.54, respectively. Our fit agrees with TEM for the largest ratio as both methods give $(T_m/R_m)_3 = 0.54$, thus we determine that the shell thickness is equal to $T \approx 34$ nm. However, the fit and TEM ratio values are getting more and more different as the shell thickness is getting thinner. In addition when imposing for T_m/R_m the value given by TEM, we could not accurately fit our data and this fit is getting worse when using

$(T_m/R_m)_1^{TEM}$. This fact is emphasized by considering the data
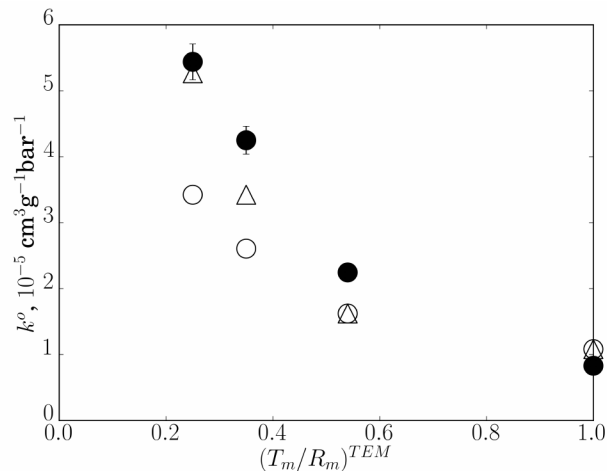

Fig. 6 Variation of the specific adiabatic compressibility of nanocapsules as measured by Pisani *et al.*[21] (●), as calculated based on Equation 24 and on T/R values derived either from TEM measurements (○) or from acoustic data fit (△).

from Pisani *et al.*[21] about the specific adiabatic compressibilities of these nanocapsules (see Figure 6). By considering as a first approximation that the nanocapsule adiabatic compressibility is the sum of the shell and core compressibilities, respectively k_s^o and k_c^o, weighted by the shell and core volume fraction, we can write:

$$k^o = \left[1 - \frac{T_m}{R_m}\right]^3 k_c^o + \left(1 - \left[1 - \frac{T_m}{R_m}\right]^3\right) k_s^o \quad (24)$$

where $k^o = 1/(K\rho)$, $K\rho$ can be either $K^s\rho^s$ or $K^c\rho^c$ depending if we want to calculate k_s^o or k_c^o. If we caculated the nanocapsule adiabatic compressibility using Equation 24 and the values $(T/R)^{TEM}$ and $(T/R)^{fit}$ we observe in Figure 6 that the $(T/R)^{fit}$ data provide a better estimation of the experimental data.

In conclusion, both the fit and TEM give the same estimation of (T_m/R_m) for a thick shell. However for thinner shells our model provides more accurate estimation than TEM data. According to the values of $(T_m/R_m)_1^{fit}$ and $(T_m/R_m)_2^{fit}$, the shell thickness is equal to 4 and 10.5 nm, respectively (while these values would have been 11.2 and 14.7 nm, respectively, based on TEM ratios).

Finally, the ratio T_m/R_m was involved in the calculation of the particle density (Equation. 2) and hence in the calculation of the nanoparticle volume fraction (Equation. 5). Since volume fractions were at first calculated from $(T_m/R_m)^{TEM}$, they became inaccurate for nanocapsules with a thin shell. Thus we have recalculated Φ using $(T_m/R_m)^{fit}$ that gives Φ^{fit} in Table 1. A further fit with Φ^{fit} did not significantly alter the previous $(T_m/R_m)^{fit}$ values.

3.6 Model predictions: Sensitivity to particle volume fraction

In Figure 8, the speed of sound and the attenuation coefficients of emulsions are displayed for the same kind of nanoparticles (with $(T_m/R_m)_1^{fit} = 0.09$) but at four volume fractions ($\phi^{fit} = 2.3$, 0.77, 0.38, and 0.08%, respectively) obtained after dilution of the most

concentrated solution. The model was plotted with no unknown parameters as we used for the remaining parameters those obtained previously from the ultrasonic curve fits (see Table 1). We observed a good agreement between the experimental data
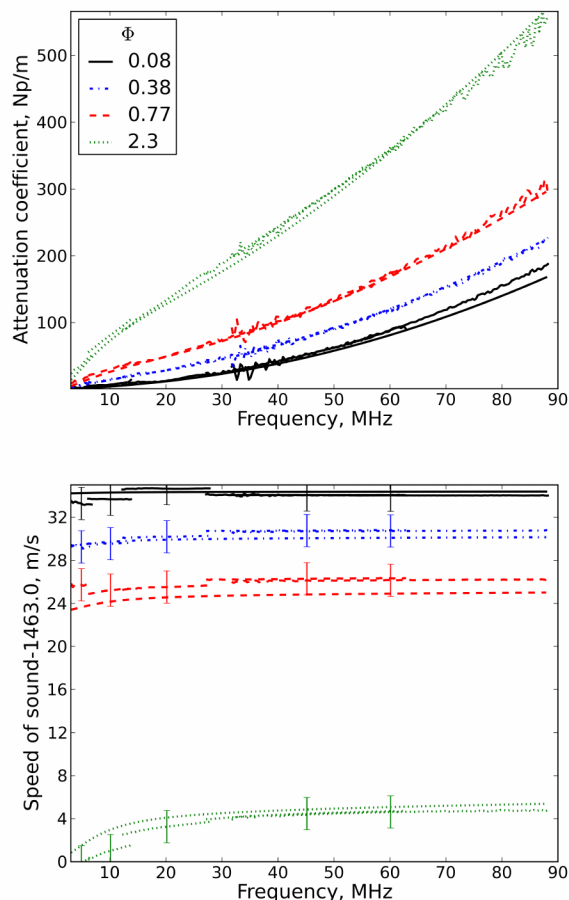

Fig. 7 Variation of the attenuation coefficient (top) and velocity (bottom) as a function of frequency for suspensions of nanoparticles ($R_m = 45$ nm) at four volume fractions: 2.3% (green), 0.77% (black), 0.38% (red), and 0.08% (blue). Noisy curves are from experimental data while smooth curves are calculated from the model with no unknown parameters left.

and the fit values. The differences in experimental sound velocity curves are small between suspensions and pure water because the liquid core and the rather stiff shell of the particles make them just slightly more compressible than water. More dilute suspensions would lead to an acoustical behavior too close to the water to be discernable. Thus, to observe the effect of geometrical and viscoelastic properties the volume fraction should be of the order of a few percents. For dilute suspensions, *i.e.* weak multiple scattering in the range of validity of the Independent Scattering Approximation[40], both effects (dilational and translational) are proportional to the particles volume fraction. This linear dependence is validated experimentally on Figure 7, for both the phase velocity and attenuation coefficient.
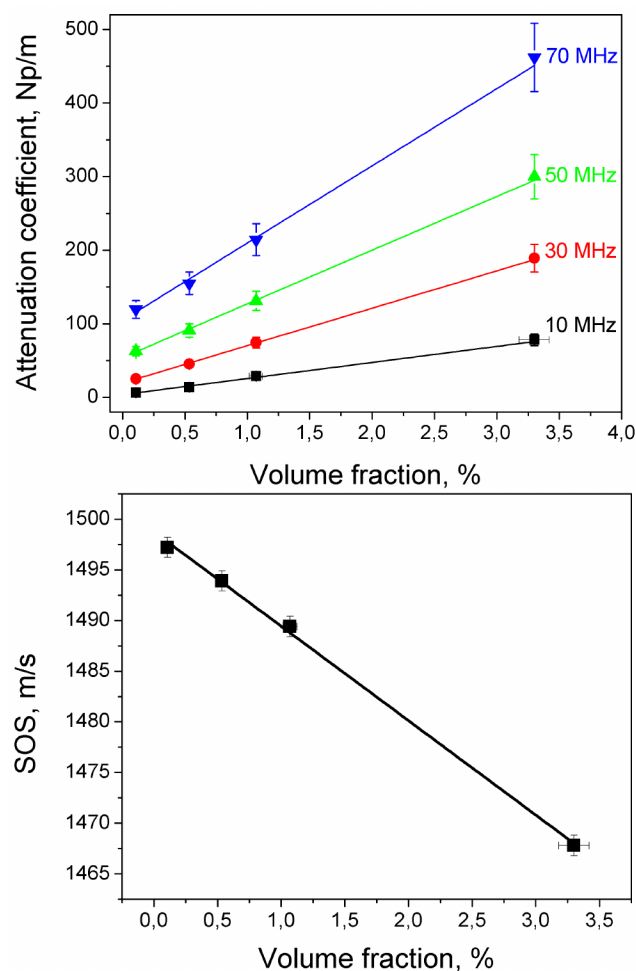

Fig. 8 Variation of the attenuation coefficient (top) and speed of sound (bottom) for suspensions containing particles at a volume fraction ranging from 0.25 to 3.2%, with radius of 45 nm and having the thinnest shell. Attenuation coefficient was taken from the spectra at several frequencies: 10 (black squares), 30 (red circles), 50 (green triangles), and 70 MHz (blue triangles). Speed of sound was taken at 50 MHz where there was no dispersion.

3.7 Model predictions: Sensitivity to geometrical parameters r and R

Since the variations in both sound velocity and attenuation are more pronounced for concentrated nanoparticle suspensions, we focus our discussion for suspensions at a volume fraction $\Phi^{fit} = 2.3$ %. We also consider nanoparticles exhibiting the thinnest shell, *i.e.* $(T_m/R_m)_1^{fit} = 0.09$. The model is then used with the same rheological parameters as previously determined to calculate the sound velocity and attenuation for various particle radii and relative thicknesses.

Our calculations show that sound velocity is rather independent of the particle radius (data not shown), while attenuation coefficient strongly depends on it (see top plot of Figure 9). In the latter case the main impact of size variation lies at medium and high frequencies and originates from the contribution of translational effect. We also observe that a variation as low as 7% in mean radius can still be detectable (*i.e.* by comparing the curve calculated for $R_m = 51$ and 55 nm). Meanwhile, the shell thick-

ness (and hence the relative shell thickness) strongly influences sound velocity. From the bottom curve in Figure 9, we calculate that a 10% change in T_m/R_m value induces a 2 m/s change in sound velocity, which is just above the typical error of our experimental set-up.

We conclude that when all the other parameters used in our model are known, acoustical spectroscopy can simultaneously measure relative thickness with an error of no less than 10% using sound velocity and the value of mean radius with a precision better than 7% using ultrasonic attenuation.
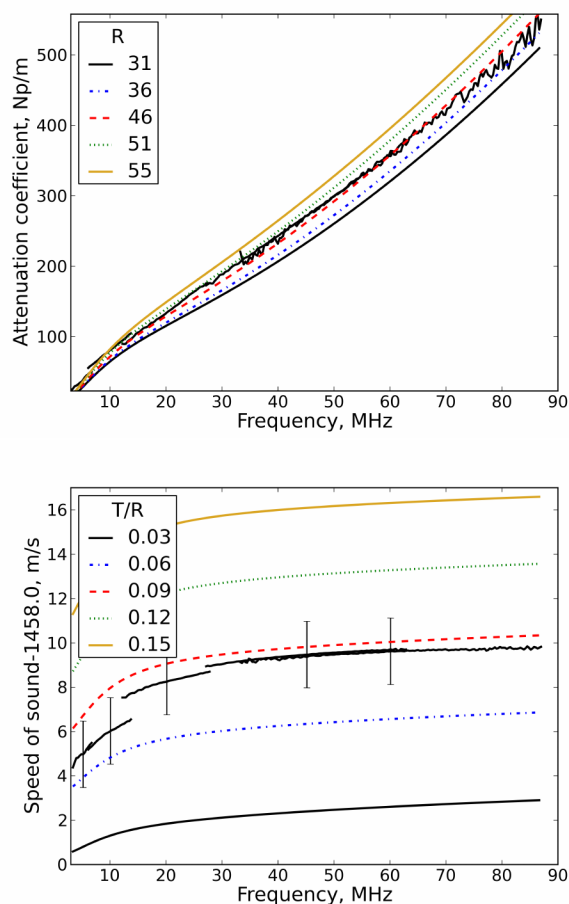

Fig. 9 Sensitivity to size (top) and relative thickness (bottom) of a suspension PLGA-PFOB nanoparticles at a volume fraction of 2.3%. Top) Attenuation coefficient of nanoparticles with $T_m/R_m = 0.09$ but having different radii: $R_m = 31$ nm (solid black), 36 nm (dashed blue), 46 nm (dashed red), 51 nm (dotted green curve), and 55 nm (solid goldenrod). Bottom) Magnitude of sound velocity in suspension of nanoparticles with a radius of $R_m = 45$ nm but with different thickness-to-radius ratio: $T_m/R_m = 0.03$ (solid black line), 0.06 (blue dots), 0.9 (dashed red), 0.12 (dotted green), 0.15 (goldenrod solid line). The noisy black curve is from experimental data.

3.8 Complexity and underlying mechanisms of ultrasound-particle interaction

We used a complex model to fit our data and we can legimately wonder if a simpler model could have also accurately fitted our experimental data. So, in the following we will justify its use with

an emphasize on the impact of all the major scattering mechanisms. To do so, we start by fitting our experimental data by the simplest model and then by using more complexe ones. We use as reference data our ultrasonic measurements performed on suspensions made of nanocapsules with the thinnest shell, $(T_m/R_m)_1^{fit} = 0.09$, and at a volume fraction of $\Phi^{fit} = 2.3\%$ as these conditions were the most sensitive to the influence of nanocapsule properties.

The most popular model describing volumetric oscillations of microbubbles with a thick shell, is the Church model[14]. This model modifies the well-known Rayleigh-Plesset equation of radial vibrations of a free bubble to take into account the influence of a viscoelastic and incompressible shell with a Kelvin-Voigt constitutive relation. In Figure 10, the green dotted curves are a fit of our data using Church model and all the viscoelastic parameters previously defined (shell viscosity, frequency-independent in this model, was 1 Pa s), and a mean radius of 42 nm. In this case, the fit gives a very small value for the relative thickness: $T_m/R_m = 0.03$. Since Church model only takes into account dilatational mechanism, it predicts that the attenuation coefficient behaves as the square of the ultrasonic frequency while the sound velocity is frequency-independent. Obviously, this model can not describe our experimental data. Although dilatational mode is dominant in the case of bubbles where the gaseous core is highly compressible, nanoparticles with a rather thick polymeric shell and a liquid core are much less deformable. Thus, this mechanism cannot be considered as the prevalent one. It is also known that viscoinertial translational effects determine the acoustical behavior of a suspension of rigid particles in the medical frequency range[9].

We have recently developed a model that describes the ultrasound dispersion and attenuation in dilute suspensions of nanometric particles by taking into account both above-mentioned effects (the dilatational mode is based on a generalized Church model).[19] In this model the nanoparticles with an incompressible shell (Kelvin-Voigt rheological behavior) are dispersed in a continuous medium. Translational effect, described using Faxén formula, induces more linear behavior of the attenuation coefficient with small dispersion in sound velocity at low frequencies. The fit of this model, containing both effects, is represented as blue dash-dot curves in Figure 10. Taking the shear viscosity of the PLGA shell as 0.1 Pa.s, the fit gives this time a relative thickness equal to $T_m/R_m = 0.04$, that is again a too small value. As for the Church model, this model fails to correctly predict the ultrasonic behavior of our nanoparticle suspensions. Even though the addition of a translational effect induces a more linear behavior in the attenuation coefficient, the calculated attenuation curve is far from the experimental one, and the model can not describe the observed dispersion in speed of sound at low frequencies.

The previous models are based on the assumption that the nanoparticle are incompressible but our viscoelastic picosecond measurements show that it is not the case. Indeed, on the one hand the PLGA Poisson's ratio is 0.36 and on the other hand the bulk modulus for PLGA is about ten times larger than for PFOB (7.3 and 0.74 GPa, respectively). In addition, PLGA is known to be an amorphous polymer undergoing a glass transition temper-
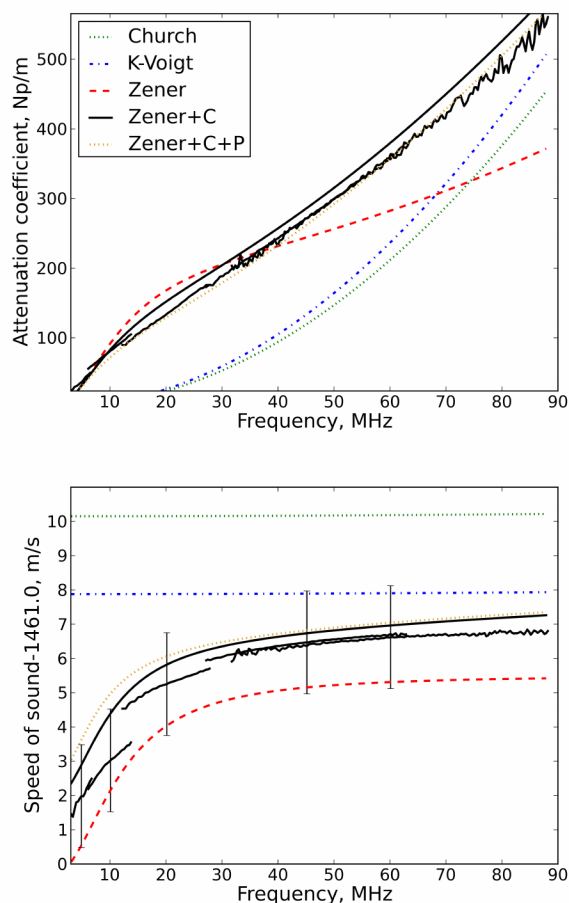
Fig. 10 Comparison of the Church and our models including translational effect fitted to data from a typical experiment with 2.3% v/v PLGA/PFOB capsules. The Church model (dotted green curves) includes only radial vibrations of the nanoparticle in the acoustical field and predicts quadratic dependence of the attenuation coefficient with the frequency, while the sound celerity stays independent of the frequency. The three other models include viscoinertial mechanism of the ultrasound attenuation besides the dilatational one and describe viscoelastic shell as a Kelvin-voigt (blue dash) and Zener material (red and black). Both our models including Zener relaxation with (solid black lines) and without (dashed red curves) compressibility of the shell reproduce the flex of the attenuation curve at approximately 10–15 MHz and the dispersion of the C lasting up to the same frequencies. But only the model that includes the compressibility and the polydispersities in size and thickness (goldenrod dotted curves) enables to keep the relative thickness of the studied capsules close to the expected one. The noisy black curve is from experimental data.

ature. Thus a predictable model may require a more complex rheology description with one or several relaxation processes.

In a latter model[20] that was used in this article, the dilationnal mode was modified by modeling the shell as a compressible material of Zener rheological type. As only one single characteristic frequency (inflection point) was observed in our experimental curves in the 10-15 MHz range, we introduced only one single relaxation process of Zener type with a relaxation angular frequency, $\omega_r = 12$ MHz in our case. Assuming an incompressible shell with one relaxation process, both translational effects and

shell rheology induce a dispersion of the velocity at low frequencies. However, this modification fails to correctly fit the experimental data as shown by the red dashed lines in Figure 10, where only T_m/R_m is an unknown parameter. If in addition we take into account shell compressibility into the model, we obtain a good fit (black lines) for sound velocity and a correct one for attenuation where the general trend of both ultrasonic parameters are well described (for $T/R = 0.06$). Finally, a better fit is obtained, especially for sound attenuation, by adding the particle radius and shell thickness dispersities (goldenrod dotted lines), in this case $T_m/R_m = 0.09$.

In our model, the dilatational effect is mostly governed by the core compressibility and the shell relative thickness T/R. It is the main effect responsible for the global decrease in speed of sound, since PFOB is less compressible than water (see Table 1). Meanwhile, the translational effect is governed by the density contrast between the particle and the surrounding fluid, thus the particle radius is an important parameter. But since this contrast depends on shell and core densities, the shell relative thickness also plays an indirect but important part in this effect. This effect is partly responsible for the frequency dependence of the speed of sound and is mainly responsible for the attenuation behavior. In addition, both attenuation and speed of sound amplitudes are also strongly dependent on volume fraction but do not depend significantly on the other parameters (than ϕ, R and T/R) that only slightly alter the ultrasonic curve shapes.

4 Conclusions

We have proposed a method using acoustic spectroscopy and a recent model that allows to extract *in vitro* physical properties of nanoparticles in suspensions when the particle volume fraction is at least of a few percents. This model shows that attenuation is mostly dependent on the particle size R while the speed of sound is rather dependent on the relative shell thickness T/R. As an example we could determine the shell thickness and its polydispersity, the shell bulk to shell viscosity ratio ζ_s/μ_s, and the shell resonance frequency of nanometric PLGA/PFOB particles. The technique is based on measuring the frequency-dependent attenuation and speed of sound of the sample with subsequent modeling. The ultrasound transmission through a dilute suspensions of nanoparticles with a liquid core has been modeled by combining i) a dilatational mode of oscillations assuming a compressible shell with a viscoelastic behavior of Zener type, and ii) a translational mode of oscillations induced by viscoinertial interaction with the continuous phase. We demonstrated that this model fits with a good accuracy our experimental data compared to other known models. Using this approach, structural or viscoelastic parameters of nanoparticules in suspension can be determined if the total number of unknown parameters is small enough. In the particular case investigated here, we were able to determine thickness parameters (mean value and distribution), with T_m/R_m values down to 0.09, thus corresponding to a mean thickness as low as 4 nm. Moreover, the proposed method is to our knowledge the only one providing an estimation of the dispersion for thickness at such nanoscales.

5   acknowledgement

References

1 R. Saidur, S. Kazi, M. Hossain, M. Rahman and H. Mohammed, *Ren. Sust. En. Rev.*, 2011, **15**, 310–323.

2 N. Arora, S. Agarwal and R. Murthy, *Int. J. Pharm. Sci. Drug Res.*, 2012, **4**, 168–182.

3 E. Lasoǹ and J. Ogonowski, *CHEMIK*, 2011, **65**, 960–967.

4 M. Díaz and P. Vivas-Mejia, *Pharmaceuticals*, 2013, **6**, 1361–1380.

5 A. Schröder and E. Raphael, *EuroPhys. Lett.*, 1992, **17**, 565–570.

6 G. Y. Yu, V. L. Newhouse and J. Satrapa, *J. Acoust. Soc. Am.*, 1988, **84**, 771–779.

7 V. Buckin and S. Kumar, *Microemulsions - An Introduction to Properties and Applications*, InTech, 2012.

8 R. A. Roy and R. E. Apfel, *J. Acoust. Soc. Am.*, 1990, **87**, 2332–2341.

9 M. Baudoin, J.-L. Thomas, F. Coulouvrat and C. Chanéac, *J. Acoust. Soc. Am.*, 2011, **129**, 1209–1220.

10 P. S. Epstein and R. R. Carhart, *J. Acoust. Soc. Am.*, 1953, **25**, 553–565.

11 J. R. Allegra and S. A. Hawley, *J. Acoust. Soc. Am.*, 1972, **51**, 1545–1564.

12 M. Baudoin, J.-L. Thomas, F. Coulouvrat and D. Lhuillier, *J. Acoust. Soc. Am.*, 2007, **121**, 3386–3397.

13 A. H. Harker and J. a. G. Temple, *J. Phys. D: Appl. Phys.*, 1988, **21**, 1576–1588.

14 C. C. Church, *J. Acoust. Soc. Am.*, 1995, **97**, 1510–1521.

15 A. A. Doinikov and P. A. Dayton, *J. Acoust. Soc. Am.*, 2007, **121**, 3331–3340.

16 P. Marmottant, A. Bouakaz, N. de Jong and C. Quilliet, *J. Acoust. Soc. Am.*, 2011, **129**, 1231–1239.

17 R. Gatignol, *J. Mécanique Théorique Appliquée*, 1983, **1**, 143–160.

18 P. Mazur and D. Bedeaux, *Physica*, 1974, **76**, 235–246.

19 F. Coulouvrat, J.-L. Thomas, K. Astafyeva, N. Taulier, J.-M. Conoir and W. Urbach, *J. Acoust. Soc. Am.*, 2012, **132**, 3748–3759.

20 M. Guédra, T. Valier-Brasier, J.-M. Conoir, F. Coulouvrat, K. Astafyeva and J.-L. Thomas, *J. Acoust. Soc. Am.*, 2014, **135**, 1044–1055.

21 E. Pisani, N. Tsapis, B. Galaz, M. Santin, R. Berti, N. Taulier, E. Kurtisovski, O. Lucidarme, M. Ourevitch, B. T. Doan, J. C. Beloeil, B. Gillet, W. Urbach, S. L. Bridal and E. Fattal, *Adv. Funct. Mat.*, 2008, **18**, 2963–2971.

22 R. Díaz-López, N. Tsapis, D. Libong, P. Chaminade, C. Connan, M. M. Chehimi, R. Berti, N. Taulier, W. Urbach, V. Nicolas and E. Fattal, *Biomaterials*, 2009, **30**, 1462–1472.

23 O. Diou, N. Tsapis, C. Giraudeau, J. Valette, C. Gueutin, F. Bourasset, S. Zanna, C. Vauthier and E. Fattal, *Biomaterials*, 2012, **33**, 5593–5602.

24 A. K. Iyer, G. Khaled, J. Fang and H. Maeda, *Drug Discov. Today*, 2006, **11**, 812–818.

25 H. Maeda, J. Wu, T. Sawa, Y. Matsumura and K. Hori, *J. Control. Release*, 2000, **65**, 271–284.

26 H. Hashizume, P. Baluk, S. Morikawa, J. W. McLean, G. Thurston, S. Roberge, R. K. Jain and D. M. McDonald, *Am. J. Pathol.*, 2000, **156**, 1363–1380.

27 F. Yuan, M. Dellian, D. Fukumura, M. Leunig, D. A. Berk, V. P. Torchilin and R. K. Jain, *Cancer Res.*, 1995, **55**, 3752–3756.

28 N. Y. Rapoport, A. M. Kennedy, J. E. Shea, C. L. Scaife and K.-H. Nam, *J. Control. Release*, 2009, **138**, 268–276.

29 P. F. Jiao, H. Y. Zhou, L. X. Chen and B. Yan, *Curr. Med. Chem.*, 2011, **18**, 2086–2102.

30 E. Pisani, N. Tsapis, J. Paris, V. Nicolas, L. Cattel and E. Fattal, *Langmuir*, 2006, **22**, 4397–4402.

31 K. Astafyeva, *PhD thesis*, 2014.

32 M. G. Freire, A. G. M. Ferreira, I. M. A. Fonseca, I. M. Marrucho and J. A. P. Coutinho, *J. Chem. Eng. Data*, 2008, **53**, 538–542.

33 N. G. Parker, M. L. Mather, S. P. Morgan and M. J. W. Povey, *Biomed. Mater.*, 2010, **5**, 055004.

34 T. Dehoux, N. Tsapis and B. Audoin, *Soft Matter*, 2012, **8**, 2586–2589.

35 K. V. de Velde and P. Kiekens, *Polymer Testing*, 2002, **21**, 432–442.

36 S. H. Choi and T. G. Park, *J. Biomat. Sci.*, 2002, **13**, 1163–1173.

37 L. Leung, C. Chan, S. Baek and H. Naguib, *Biomed. Mater.*, 2008, **3**, 025006.

38 M. H. Lee and D. Lee, *Soft Matter*, 2010, **6**, 4326–4330.

39 A. Lejardi, A. E. López, J. R. Sarasua, U. B. Sleytr and J. L. Toca-Herrera, *J. Chem. Phys.*, 2013, **139**, 121903.

40 L. L. Foldy, *Phys. Rev.*, 1945, **67**, 107–119.